Error-transparent operations on a logical qubit protected by quantum error correction

Y. Ma,[1] Y. Xu,[1] X. Mu,[1] W. Cai,[1] L. Hu,[1] W. Wang,[1] X. Pan,[1] H. Wang,[1] Y. P. Song,[1] C.-L. Zou,[2, *] and L. Sun[1, †]

[1]*Center for Quantum Information, Institute for Interdisciplinary Information Sciences, Tsinghua University, Beijing 100084, China*
[2]*Key Laboratory of Quantum Information, CAS, University of Science and Technology of China, Hefei, Anhui 230026, P. R. China*

Universal quantum computation [1] is striking for its unprecedented capability in processing information, but its scalability is challenging in practice because of the inevitable environment noise. Although quantum error correction (QEC) techniques [2–7] have been developed to protect stored quantum information from leading orders of errors, the noise-resilient processing of the QEC-protected quantum information is highly demanded but remains elusive [8]. Here, we demonstrate phase gate operations on a logical qubit encoded in a bosonic oscillator in an error-transparent (ET) manner. Inspired by Refs. [9, 10], the ET gates are extended to the bosonic code and are able to tolerate errors during the gate operations, regardless of the random occurrence time of the error. With precisely designed gate Hamiltonians through photon-number-resolved AC-Stark shifts, the ET condition is fulfilled experimentally. We verify that the ET gates outperform the non-ET gates with a substantial improvement of the gate fidelity after an occurrence of the single-photon-loss error. Our ET gates in the superconducting quantum circuits are readily for extending to multiple encoded qubits and a universal gate set is within reach, paving the way towards fault-tolerant quantum computation.

The uncontrollable noise in a quantum system is the most significant obstacle in realizing universal quantum computation [1], since the induced errors are unpredictable and deleterious to the encoded quantum information. Quantum error correction (QEC) is proposed to tackle this problem [11] by expanding the dimension of the Hilbert space for quantum information and thus introducing the redundancy to tolerate the leading errors. In conventional QEC, quantum information is encoded on logical qubits, constructed by multiple physical qubits, within a subspace spanned by the QEC codewords called the code space. Although each physical qubit is susceptible to noise, errors can be detected without corrupting the stored quantum information while mapping the quantum state in the code space to the orthogonal error spaces. Over the past years, great progress has been achieved in QEC theories, and proof-of-principle demonstrations of error detection and correction are reported in various experimental platforms [2–7]. Especially, the break-even point of QEC has been demonstrated with a logical qubit encoded in a bosonic oscillator [12].

However, QEC can merely maintain the stored quantum states from noise. Errors occurring during the execution of quantum operations might accumulate and spread over the quantum circuits, so that the processing of information is not reliable. Fault-tolerant universal quantum computation architectures [8], such as the transversal gates on logical qubits and magic-state distillation, were developed for performing noise-resilient quantum gates on encoded qubits, but the implementations are extremely challenging. Instead of realizing a complete fault-tolerant architecture, practical schemes that demonstrate the key ideas in a near-term few-qubit system were proposed [13, 14]. Only very recently, fault-tolerant state preparation [15] and error detection [16, 17] were experimentally demonstrated. An alternative approach of fault-tolerant operations based on the concept of error-transparent (ET) gates [9, 10] was proposed theoretically and promises fault-tolerant non-Clifford logical gates. Nevertheless, its implementation in the multi-qubit QEC codes requires many-
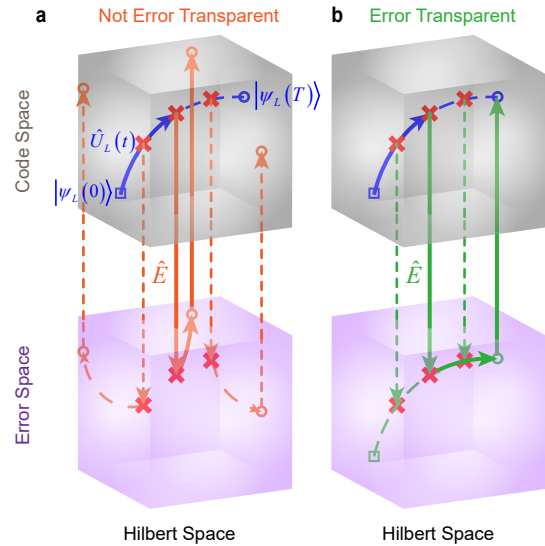

FIG. 1. **Concept of error-transparent (ET) gate.** During a quantum gate on a logical state with finite operation time, error E might occur randomly, mapping the state in the code space (upper gray cube) to the orthogonal error space (lower purple cube). For the non-ET gate (**a**), the track of state evolution in the error space is different for E occurring at different time. When the ET condition is satisfied (**b**), the tracks in both the code and error spaces are deterministic and identical whenever the error occurs. Therefore, E can be detected and corrected with QEC after the gate operation, making the ET gate fault tolerant.

body interactions and is hard to realize experimentally.

Here, we extend the concept of ET gates to bosonic QEC codes and experimentally demonstrate ET arbitrary phase gates that tolerate the single-photon-loss error. The ET gates are successfully validated by the remarkable improvement of the coherence of the logical states after the occurrence of an error during the evolution of the gates. By applying repetitive autonomous QEC (AQEC), the ET gates on the QEC-protected logical qubits show higher fidelities than the cases

with non-ET gates or without AQEC. Our results promise a universal ET gate set for quantum computation, thus reveals the potential of the bosonic quantum computation architecture [18, 19], and presents a first step towards the fault-tolerant quantum computation.

The basic idea of the ET operation on a logical qubit is illustrated in Fig. 1. Applying a Hamiltonian $H(t)$ to the logical qubit, any encoded quantum state is expected to evolve as $|\psi_{\rm L}(t_1)\rangle \rightarrow U(t_2,t_1)|\psi_{\rm L}(t_1)\rangle$ with a target unitary operation $U(t_2,t_1) = \mathscr{T} e^{-i\int_{t_1}^{t_2} d\tau H(\tau)}$ ($\mathscr{T}$ is the time-ordering operator). However, because errors could occur during the operation process, the logical state will consequently jump from the code space to the error space. Due to the stochastic nature of noise, the practical evolution of the state may follow different tracks, as shown in Fig. 1a. For example, if an error E_j occurs at time t, the track leads to the final state $|\widetilde{\psi}(t)\rangle = U(T,t)E_jU(t,0)|\psi_{\rm L}(0)\rangle$ in the error space. An ET operation requires a deterministic track of the logical state evolution irrespective to t, as shown in Fig. 1b, and the target operation could always be achieved by mapping the state back to the code space after the operation.

Therefore, we derive the condition for the ET operation as $U(T,t)E_jU(t,0)|\psi_{\rm L}(0)\rangle = e^{i\phi(t)}E_jU(T,0)|\psi_{\rm L}(0)\rangle, \forall j,t, |\psi_{\rm L}(0)\rangle$ by considering the fact that a global phase $\phi(t)$ makes no influence on the logical state. Note that the ET condition discussed in Refs. [9, 10] is a more restricted case of our condition with $\phi(t) = 0$. Accordingly, the Hamiltonian should be carefully engineered to make the evolution in the error spaces exactly the same as that in the code space, i.e.

$$\mathscr{P}_j^\dagger H(t)\mathscr{P}_j = \mathscr{P}_{\rm C}^\dagger H(t)\mathscr{P}_{\rm C} + c(t)\mathscr{P}_{\rm C}, \forall j,t, \qquad (1)$$

where $\mathscr{P}_{\rm C}$ is the projector onto the code space, $\mathscr{P}_j \propto E_j\mathscr{P}_{\rm C}$ is the projector from the code space to the error space corresponding to the error E_j, and $c(t)$ is a complex number.

To demonstrate the ET operations on a bosonic logical qubit, we explore a superconducting circuit consisting of a high-quality microwave cavity constituting the bosonic logical qubit and a dispersively coupled transmon qubit as the ancilla [20, 21], and the system Hamiltonian reads

$$H_0 = \Delta\omega a^\dagger a - \chi a^\dagger a |e\rangle\langle e| - \frac{K}{2}a^{\dagger 2}a^2. \qquad (2)$$

Here, $\Delta\omega$ is the cavity frequency with respect to a carefully chosen local oscillator reference, $a^\dagger$ (a) is the creation (annihilation) operator for the bosonic mode, $|e\rangle$ ($|g\rangle$) is the excited (ground) state of the ancilla, and $\chi/2\pi = 1.60$ MHz and $K/2\pi = 4.80$ kHz are the dispersive coupling and Kerr coefficients originated from the ancilla, respectively. To correct the dominant photon-loss errors in the bosonic mode, we encode the quantum information on the lowest-order binomial code in the cavity [22, 23], which is defined in Fock basis as

$$|0_{\rm L}\rangle = \frac{|0\rangle + |4\rangle}{\sqrt{2}}, |1_{\rm L}\rangle = |2\rangle. \qquad (3)$$

We note that proper reference frame needs to be carefully chosen such that there is no accumulation of the relative phase between Fock states $|0\rangle$ and $|4\rangle$. When a single-photon-loss error occurs, the quantum state jumps into the error space spanned by the basis states

$$|0_{\rm E}\rangle = |3\rangle, |1_{\rm E}\rangle = |1\rangle. \qquad (4)$$

When prepare the logical qubit in the code space and set the ancilla to the idle state $|g\rangle$, a phase operation on the logical qubit can be easily realized via the Kerr effect since

$$\mathscr{P}_{\rm C}^\dagger H_0 \mathscr{P}_{\rm C} = K(I - Z) \qquad (5)$$

with respect to the code basis states (Eq. 3). Here, I and Z are the Pauli matrices. Thus, an arbitrary phase gate $R_{\rm Kerr}(\phi) = e^{i\frac{1}{2}\phi Z}$ on a single logical qubit can be implemented by waiting for a duration of $\tau = \phi/2K$. However, such phase operations can not tolerate single-photon-loss errors, because the ET condition is not satisfied as

$$\mathscr{P}_{\rm E}^\dagger H_0 \mathscr{P}_{\rm E} = \frac{3}{2}KI. \qquad (6)$$

Furthermore, the cavity's Kerr nonlinearity associated with the coupling to the ancilla cannot be switched off, therefore the stored logical qubit is always impacted by $R_{\rm Kerr}$ and suffers random photon-loss-error-induced dephasing [23].

To meet the ET condition, we develop a technique to flexibly engineer the Hamiltonian in both the code and error spaces. Through a detuned microwave drive on the ancilla, photon-number-resolved AC-Stark shift (PASS) can be realized. As schematically shown in Fig. 2a, due to the strong ancilla-cavity dispersive coupling, the transition frequency of the ancilla is photon-number (n) dependent, and thus an off-resonant drive would induce photon-number dependent energy shift δ_n due to the AC-Stark effect [24, 25]. Such a frequency shift can also be understood as a geometric phase accumulation $\sim \delta_n\tau = \frac{\Omega^2}{\Delta_{\rm d} - n\chi}\tau$ for the joint ancilla-cavity state $|gn\rangle$ (Fig. 2b), while keeping the excitation to $|en\rangle$ negligible due to the large detuning (Supplementary Information). Here τ is the gate duration time, Ω is the Rabi drive frequency, and $\Delta_{\rm d}$ is the drive detuning with respect to the ancilla transition frequency corresponding to $n = 0$. By applying drives with carefully chosen frequencies and amplitudes, we could precisely engineer the frequency shifts of the Fock states to realize the Hamiltonian

$$H_{\rm PASS} = \sum_{n=0}^{n_{\rm trc}} \delta_n |n\rangle\langle n|, \qquad (7)$$

with the truncated photon number $n_{\rm trc} = 4$ for the code considered in this work (Eq. 3 and Eq. 4). Figure 2c shows the measured Fock state frequencies when applying a continuous drive in the middle of the ancilla transition frequencies corresponding to $n = 3$ and $n = 4$, i.e. $\Delta_{\rm d} = -3.50\chi$ (the dashed orange line in Fig. 2a). The experimental results are well consistent with the theoretical predictions.
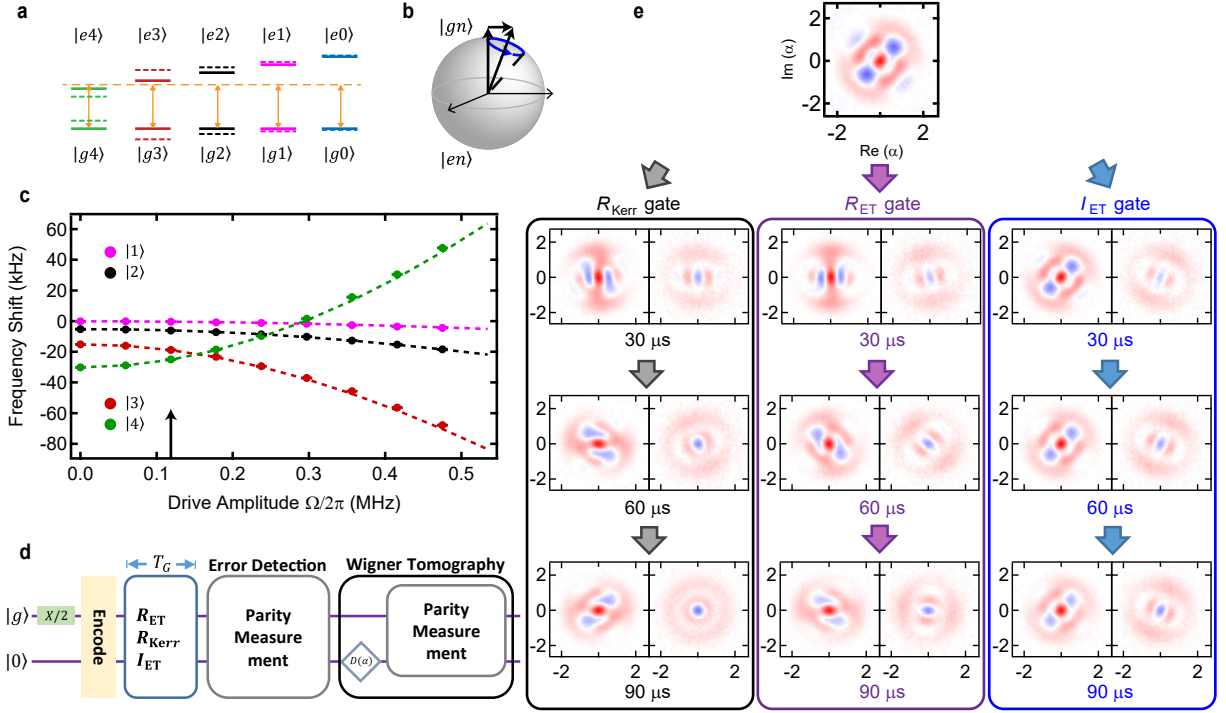
FIG. 2. **Photon-number-resolved AC-Stark shift (PASS) and ET phase gates. a,** Illustration of the energy diagram in the strongly dispersively coupled bosonic mode-ancilla system. A detuned microwave drive on the ancilla would induce PASS for each transition frequency. **b,** Geometric phase interpretation of the PASS. Fast rotating of the state in the Bloch space $\{|gn\rangle, |en\rangle\}$ induces a phase accumulation proportional to time, equivalent to an energy shift of Fock state $|n\rangle$. **c,** Measured frequencies of Fock states with respect to $|0\rangle$ as a function of the amplitude of a continuous drive. The drive frequency is in the middle of the ancilla transition frequencies corresponding to Fock states $|3\rangle$ and $|4\rangle$, as indicated by the horizontal dashed orange line in **a**. These results fit excellently with the theoretical predictions (dashed lines). The vertical arrow indicates the amplitude to realize the ET phase gate R_{ET}. **d,** Experimental sequence to characterize the ET gates. After R_{Kerr}, R_{ET}, or I_{ET}, an error detection measurement is performed, followed by a Wigner tomography. **e,** Evolution of the logical state encoded with the lowest-order binomial code $(|0_L\rangle - i|1_L\rangle)/\sqrt{2}$ under the three different gates for different intervals of 30 μs, 60 μs, and 90 μs. Each left column is the Wigner function for a detection of no error, while each right one for a detection of an error. For non-ET R_{Kerr}, the state after an error eventually loses the phase information and becomes a mixed state; while for the ET gates, the coherence of the state in the error space is preserved. All the Wigner functions are experimentally measured ones.

After experimentally validating the precisely controlled PASS, we turn to realize the ET phase gate R_{ET} on the logical qubit. With an appropriate drive amplitude, we can obtain

$$\mathscr{P}_C^\dagger(H_0 + H_{PASS})\mathscr{P}_C = K'(I - Z) \qquad (8)$$

and

$$\mathscr{P}_E^\dagger(H_0 + H_{PASS})\mathscr{P}_E = K'(I - Z) + cI, \qquad (9)$$

with $K'/2\pi = 3.33$ kHz and $c/2\pi = -0.63$ kHz. Here, the ET condition is satisfied with a re-chosen reference $\Delta\omega = 6.09$ kHz. We now verify the ET property of the phase gate by measuring the evolution of a logical state $(|0_L\rangle - i|1_L\rangle)/\sqrt{2}$ with (R_{ET}) and without (R_{Kerr}) the PASS. To separately check the quantum evolution in the code and error spaces, we perform Wigner tomography of the output states by post-selecting the parity of the excitation number after various evolution times (Fig. 2**d**) with the assistance of the ancilla [23, 26]. The results are summarized in Fig. 2**e**. Comparing R_{ET} and R_{Kerr}, the evolution of the logical state in the

code space shows similar rotations and phase coherence for both cases, as indicated by the fringes in the azimuth direction. However, the phase coherence in the error space is only preserved by R_{ET}, in strong contrast to the significant corruption of phase coherence for R_{Kerr}, manifesting the tolerance to the stochastic photon-loss error during the ET gate.

Additionally, the ET idle gate I_{ET} can also be realized by simultaneously applying two PASS drives, such that $K' = 0$. This ET realization of an idle Hamiltonian is important, since the Kerr effect could be shut off and the quantum information can be protected by the binomial QEC code from random photon-loss-error-induced dephasing. In Fig. 2**e**, I_{ET} shows similar ET properties as R_{ET}, while the phase of the logical state remains unchanged in both the code and error spaces.

To demonstrate the potential of the ET gates for fault-tolerant quantum computation, we further investigate the ET gates under AQEC protection, with the experimental sequence shown in Fig. 3**a**. An AQEC pulse numerically optimized with a duration of 1.5 μs recovers the error state during the ET gate operation and also transfers the error entropy associated with
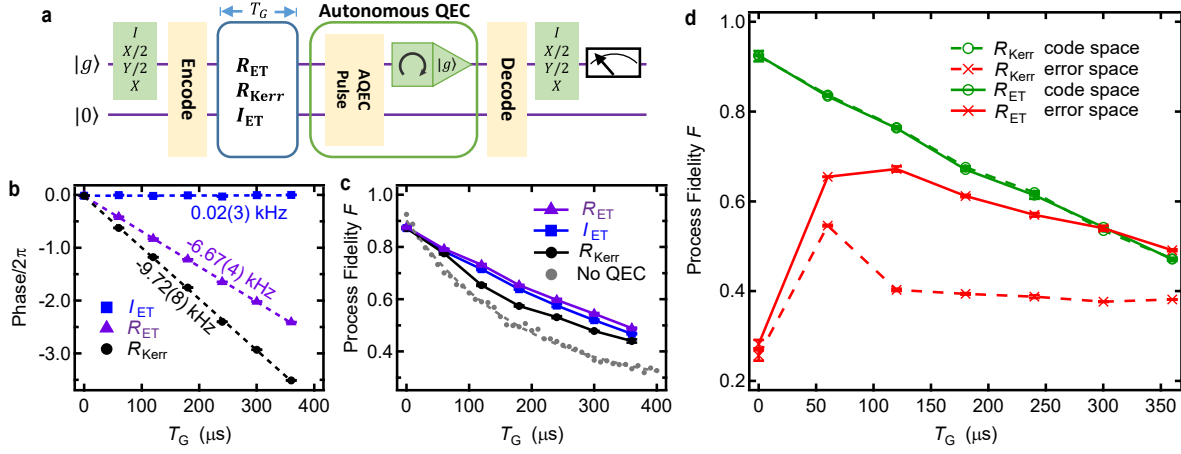
FIG. 3. **ET gates on a logical qubit with autonomous quantum error correction (AQEC). a,** Experimental procedure for the ET gate performance characterization. The gate operation on the logical qubit is realized by the corresponding Hamiltonian with varying gate time T_G, and a QEC process is implemented before the decoding. The QEC process consists of an AQEC pulse followed by an ancilla measurement and a reset. **b,** Phase shift of the logical state extracted from the process tomography. During the phase gates, the phases of the logical state change linearly with T_G. **c,** The gray dotted curve is the process fidelity F of R_{Kerr} without AQEC and could be regarded as a reference. The AQEC indeed improves F except for T_G being small. The ET gates perform better than R_{Kerr} as expected. **d,** F in the error and code spaces respectively. In the code space, both R_{Kerr} and R_{ET} have nearly identical F. However, in the error space R_{ET} has much higher F than R_{Kerr}, corroborating that the ET gate is able to protect the state when an error occurs during the gate. Note that at $T_G = 0$ there is no single-photon-loss error yet and the small probability of inferring the error space mainly comes from the imperfect AQEC pulse and ancilla excitation, consistent with numerical simulations (Supplementary Information).
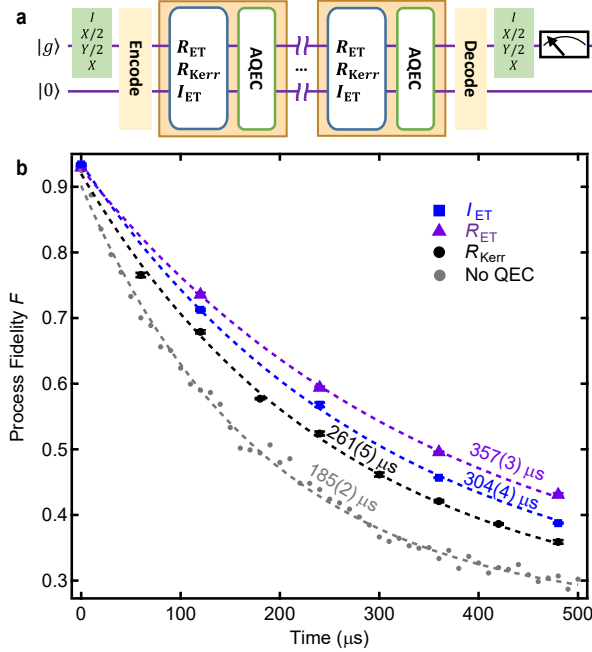

FIG. 4. **ET gates protected by repetitive AQEC. a,** Experimental sequence. **b,** Experimental process fidelity F as a function of time with repetitive and interleaved ET gates and AQECs on the logical qubit. Both ET gates have better performance than the non-ET R_{Kerr}. The lifetime with the ET idle gate I_{ET} is shorter than that with the ET phase gate R_{ET} because of extra ancilla excitation from the additional drive. All these three gates with AQEC show better performance than the case without AQEC.

the logical state to the ancilla, followed by a measurement-based ancilla reset (Methods and Supplementary Information). The AQEC is equivalent to previously demonstrated feedback-based QEC [23], but holds the advantages of convenience in experiments and avoids the latency in the electronic control system since the AQEC is error-detection free [3, 4, 6]. Figures 3**b-d** summarize the experimental results and process fidelities with different gate operation time T_G. Arbitrary phase gates can be achieved with appropriate T_G, however their gate fidelities F decay with T_G as expected. In Fig. 3**c**, we find all the gates are improved by AQEC when compared with R_{Kerr} without AQEC, while the ET gates show superior performances. By measuring the process fidelity F in the code and error spaces separately, the ET effect is clearly evidenced in Fig. 3**d**: F for R_{Kerr} and R_{ET} in the code space are almost identical, but F for R_{ET} in the error space is substantially improved.

Finally, the ET logical gate can be interleaved with AQEC and performed repeatedly, as illustrated in Fig. 4**a**. Figure 4**b** shows the measured process fidelity decaying exponentially as a function of time. We have chosen the optimal time interval for each gate (60 μs for R_{Kerr} and 120 μs for the ET gates). Clearly, both ET gates have better performance than the non-ET R_{Kerr}. The lifetime with I_{ET} is shorter than that with R_{ET} because of extra ancilla excitation from the additional drive, which causes dephasing of the logical state. In addition, all these three gates with AQEC have better performance than the case without AQEC, demonstrating the effectiveness of AQEC.

We introduce the concept of ET gates on a bosonic logical qubit, where the evolution in the error space is independent and exactly the same as that in the code space. The ET arbitrary phase gates and the idle gate have been demonstrated on the lowest-order binomial code by engineering the frequency shift of each Fock state, and an enhancement on the ET gate fidelity has also been demonstrated with repetitive AQEC. Our approach could also be generalized to single-qubit Hadamard gate and controlled-phase gate on two binomial logical qubits (Supplementary Information), thus constituting the universal ET gate set for quantum computation. Therefore, the ET gates and the bosonic QEC codes offer an alternative fault-tolerant quantum computation architecture. We note that another ET gate on a bosonic logical qubit was independently demonstrated in [27], which tolerates the damping error of the ancilla by exploiting the ancilla's higher energy levels. These two ET gate demonstrations are complementary and together promise the ET implementation of QEC against both the damping error of the ancilla and photon-loss error of the bosonic mode.

----

* clzou321@ustc.edu.cn
† luyansun@tsinghua.edu.cn

[1] M. A. Nielsen and I. L. Chuang, *Quantum Computation and Quantum Information* (Cambridge Univ. Press, 2000).

[2] J. Chiaverini, D. Leibfried, T. Schaetz, M. D. Barrett, R. B. Blakestad, J. Britton, W. M. Itano, J. D. Jost, E. Knill, C. Langer, R. Ozeri, and D. J. Wineland, "Realization of quantum error correction." Nature **432**, 602 (2004).

[3] P. Schindler, J. T. Barreiro, T. Monz, V. Nebendahl, D. Nigg, M. Chwalla, M. Hennrich, and R. Blatt, "Experimental Repetitive Quantum Error Correction," Science **332**, 1059 (2011).

[4] M. D. Reed, L. DiCarlo, S. E. Nigg, L. Sun, L. Frunzio, S. M. Girvin, and R. J. Schoelkopf, "Realization of three-qubit quantum error correction with superconducting circuits," Nature **482**, 382 (2012).

[5] X.-C. Yao, T.-X. Wang, H.-Z. Chen, W.-B. Gao, A. G. Fowler, R. Raussendorf, Z.-B. Chen, N.-L. Liu, C.-Y. Lu, Y.-J. Deng, Y.-A. Chen, and J.-W. Pan, "Experimental demonstration of topological error correction." Nature **482**, 489 (2012).

[6] G. Waldherr, Y. Wang, S. Zaiser, M. Jamali, T. Schulte-Herbrüggen, H. Abe, T. Ohshima, J. Isoya, J. F. Du, P. Neumann, and J. Wrachtrup, "Quantum error correction in a solid-state hybrid spin register." Nature **506**, 204 (2014).

[7] J. Kelly, R. Barends, A. G. Fowler, A. Megrant, E. Jeffrey, T. C. White, D. Sank, J. Y. Mutus, B. Campbell, Y. Chen, Z. Chen, B. Chiaro, A. Dunsworth, I.-C. Hoi, C. Neill, P. J. J. O'Malley, C. Quintana, P. Roushan, A. Vainsencher, J. Wenner, A. N. Cleland, and J. M. Martinis, "State preservation by repetitive error detection in a superconducting quantum circuit," Nature **519**, 66 (2015).

[8] E. T. Campbell, B. M. Terhal, and C. Vuillot, "Roads towards fault-tolerant universal quantum computation," Nature **549**, 172 (2017).

[9] O. Vy, X. Wang, and K. Jacobs, "Error-transparent evolution: the ability of multi-body interactions to bypass decoherence," New J. Phys. **15**, 053002 (2013).

[10] E. Kapit, "Error-transparent quantum gates for small logical qubit architectures," Phys. Rev. Lett. **120**, 050503 (2018).

[11] P. Shor, "Scheme for reducing decoherence in quantum computer memory," Phys. Rev. A **52**, 2493 (1995).

[12] N. Ofek, A. Petrenko, R. Heeres, P. Reinhold, Z. Leghtas, B. Vlastakis, Y. Liu, L. Frunzio, S. Girvin, L. Jiang, *et al.*, "Extending the lifetime of a quantum bit with error correction in superconducting circuits," Nature **536**, 441 (2016).

[13] D. Gottesman, "Quantum fault tolerance in small experiments," arXiv:1610.03507 (2016).

[14] R. Chao and B. W. Reichardt, "Fault-tolerant quantum computation with few qubits," npj Quantum Inf. **4**, 42 (2018).

[15] M. Takita, A. W. Cross, A. D. Córcoles, J. M. Chow, and J. M. Gambetta, "Experimental Demonstration of Fault-Tolerant State Preparation with Superconducting Qubits," Phys. Rev. Lett. **119**, 180501 (2017).

[16] N. M. Linke, M. Gutierrez, K. A. Landsman, C. Figgatt, S. Debnath, K. R. Brown, and C. Monroe, "Fault-tolerant quantum error detection," Sci. Adv. **3**, e1701074 (2017).

[17] S. Rosenblum, P. Reinhold, M. Mirrahimi, L. Jiang, L. Frunzio, and R. J. Schoelkopf, "Fault-tolerant detection of a quantum error," Science **361**, 266 (2018).

[18] Y. Y. Gao, B. J. Lester, K. S. Chou, L. Frunzio, M. H. Devoret, L. Jiang, S. M. Girvin, and R. J. Schoelkopf, "Entanglement of bosonic modes through an engineered exchange interaction," Nature **566**, 509 (2019).

[19] C. Flühmann, T. L. Nguyen, M. Marinelli, V. Negnevitsky, K. Mehta, and J. P. Home, "Encoding a qubit in a trapped-ion mechanical oscillator," Nature **566**, 513 (2019).

[20] A. Wallraff, D. I. Schuster, A. Blais, L. Frunzio, R.-S. Huang, J. Majer, S. Kumar, S. M. Girvin, and R. J. Schoelkopf, "Strong coupling of a single photon to a superconducting qubit using circuit quantum electrodynamics," Nature **431**, 162 (2004).

[21] H. Paik, D. I. Schuster, L. S. Bishop, G. Kirchmair, G. Catelani, a. P. Sears, B. R. Johnson, M. J. Reagor, L. Frunzio, L. I. Glazman, S. M. Girvin, M. H. Devoret, and R. J. Schoelkopf, "Observation of High Coherence in Josephson Junction Qubits Measured in a Three-Dimensional Circuit QED Architecture," Phys. Rev. Lett. **107**, 240501 (2011).

[22] M. H. Michael, M. Silveri, R. T. Brierley, V. V. Albert, J. Salmilehto, L. Jiang, and S. M. Girvin, "New Class of Quantum Error-Correcting Codes for a Bosonic Mode," Phys. Rev. X **6**, 031006 (2016).

[23] L. Hu, Y. Ma, W. Cai, X. Mu, Y. Xu, W. Wang, Y. Wu, H. Wang, Y. P. Song, C.-L. Zou, S. M. Girvin, L.-M. Duan, and L. Sun, "Quantum error correction and universal gate set operation on a binomial bosonic logical qubit," Nat. Phys. **15**, 503 (2019).

[24] D. I. Schuster, A. Wallraff, A. Blais, L. Frunzio, R.-S. Huang, J. Majer, S. M. Girvin, and R. J. Schoelkopf, "ac stark shift and dephasing of a superconducting qubit strongly coupled to a cavity field," Phys. Rev. Lett. **94**, 123602 (2005).

[25] O. Gamel and D. F. V. James, "Time-averaged quantum dynamics and the validity of the effective Hamiltonian model," Phys. Rev. A **82**, 052106 (2010).

[26] L. Sun, A. Petrenko, Z. Leghtas, B. Vlastakis, G. Kirchmair, K. M. Sliwa, A. Narla, M. Hatridge, S. Shankar, J. Blumoff, L. Frunzio, M. Mirrahimi, M. H. Devoret, and R. J. Schoelkopf, "Tracking photon jumps with repeated quantum non-demolition parity measurements," Nature **511**, 444 (2014).

[27] P. Reinhold, S. Rosenblum, W.-L. Ma, L. Frunzio, L. Jiang, and R. J. Schoelkopf, "Error-corrected gates on an encoded qubit," arXiv:1907.12327 (2019).

Supplementary Information for "Error-transparent operations on a logical qubit protected by quantum error correction"

Y. Ma,[1] Y. Xu,[1] X. Mu,[1] W. Cai,[1] L. Hu,[1] W. Wang,[1] X. Pan,[1] H. Wang,[1] Y. P. Song,[1] C.-L. Zou,[2, *] and L. Sun[1, †]

[1]*Center for Quantum Information, Institute for Interdisciplinary Information Sciences, Tsinghua University, Beijing 100084, China*
[2]*Key Laboratory of Quantum Information, CAS, University of Science and Technology of China, Hefei, Anhui 230026, P. R. China*

I.   EXPERIMENTAL PARAMETERS AND TECHNIQUES

A.   Experimental device

The experimental device is composed of two high-quality three-dimensional coaxial aluminum cavities [1–3] (S_1 and S_2), three ancillary transmon qubits (Q_1, Q_2, Q_3) and three stripline cavities [4] (R_1, R_2, R_3), as shown in Fig. S1. The detailed geometry of the device can be found in Ref. [5]. For current experiment on the error-transparent (ET) gates on a single-logical qubit, we only use the left part of the device (S_1, Q_1, and R_1), and the remaining parts stay in their ground states during the experiment. The single-logical qubit is encoded in the bosonic mode of S_1 (referred as the 'cavity' henceforth), which is dispersively coupled to the ancilla Q_1. The stripline cavity R_1 with a high external coupling rate (κ_{out}) is to readout Q_1. The relevant parameters and coherence properties of the device under study are listed in Table S1 and Table S2. Note that the coefficients $\chi = \chi_{qs}$ and $K = K_s$ are used in the main manuscript and below for abbreviation.

B.   Experimental techniques

In this work, we have developed two experimental techniques to realize the ET gates under the protection of repetitive quantum error correction (QEC). The first technique is the photon-number-resolved AC-Stark shift (PASS) to engineer the system Hamiltonian precisely, and thus the ET condition

Term	Value
$\omega_q/2\pi$	6.036 GHz
$\omega_s/2\pi$	6.594 GHz
$\omega_r/2\pi$	8.892 GHz
$K_q/2\pi$	252 MHz
$K_s/2\pi$	4.8 kHz
$\chi_{qs}/2\pi$	1.60 MHz
$\chi_{qr}/2\pi$	2.00 MHz

TABLE S1.   **Experimentally characterized parameters for the cavities and the ancilla qubit.** Here, the subscripts (q,s,r) denote the ancilla qubit (Q_1), storage cavity (S_1) and readout cavity (R_1), respectively. ω is the bare frequency for each compoment, K is the self-Kerr coefficient and χ is the dispersive coupling strength.

	Q_1	Q_3	S_1	R_1
T_1	35 μs	25 μs	480 μs	58 ns
T_2	25 μs	30 μs	560 μs	-
T_ϕ	39 μs	75 μs	1.3 ms	-
n_{th}	1.6%	0.7%	< 1%	-

TABLE S2.   **Coherence properties of the ancilla qubits and the cavities.** T_1 and T_2 are the experimentally measured energy and phase relaxation times, respectively, T_ϕ is the derived pure dephasing time, and n_{th} is the thermal excitation in the experiment.

can be satisfied for the binomial codes. The second technique is the autonomous QEC (AQEC), by which the single-photon-loss error can be detected and corrected without extracting the error syndrome by the control electronics and thus the electronic latency can be avoided. In this section, we provide the details of the two techniques.

1.   PASS

For the system under study, the Hamiltonian for realizing PASS reads

$$H_0 = \Delta\omega a^\dagger a - \frac{K}{2} a^{\dagger 2} a^2 + \left(\omega_q - \chi a^\dagger a - \omega_d\right) |e\rangle \langle e| + \Omega\left(|e\rangle \langle g| + |g\rangle \langle e|\right), \tag{S1}$$

where $\Delta\omega$ is the cavity frequency with respect to a carefully chosen local oscillator reference, $a^\dagger$ (a) is the creation (annihilation) operator for the bosonic mode, $|e\rangle$ ($|g\rangle$) is the excited (ground) state of the ancilla, χ is the dispersive coupling strength, K is the self-Kerr coefficient of the cavity originated
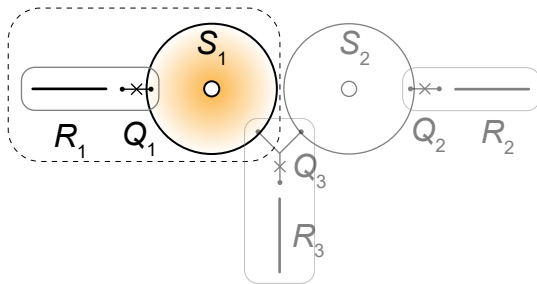

FIG. S1.   **Experimental device.** The ET gate experiment is based on the parts in the dashed rectangle, consisting of a high-quality three-dimensional coaxial aluminum cavity S_1 as the storage cavity to encode the logical qubit, an ancillary transmon qubit Q_1, and a stripline cavity R_1 for readout of the ancilla. The remaining parts are in their ground states during the experiment.
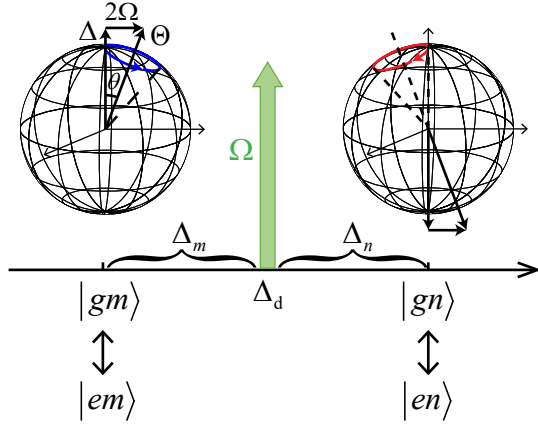
FIG. S2. **Geometric phase interpretation of the PASS.** An off-resonant drive with a frequency Δ_d between two dispersive transition frequencies of the ancilla and an amplitude Ω would produce a geometric phase on each ancilla state. This phase is accumulated constantly and causes an equivalent frequency shift on the photon Fock state because the ancilla is approximately in its ground state and can be traced out. The direction of the frequency shift is related to the sign of the detuning Δ.

from the ancilla, ω_q is the ancilla qubit frequency when the cavity is in vacuum, ω_d is the driving frequency on the ancilla, and Ω is the Rabi drive frequency. In the following, we define $\Delta_d \equiv \omega_q - \omega_d$. In the limit of $\Omega \ll |\Delta_d - \chi a^\dagger a|$ for all cavity states, we have the effective Hamiltonian as [6]

$$H_{\text{eff}} \approx \Delta\omega a^\dagger a - \frac{K}{2}a^{\dagger 2}a^2 + (\Delta_d - \chi a^\dagger a)|e\rangle\langle e|$$
$$+ \frac{\Omega^2}{(\Delta_d - \chi a^\dagger a)}(|e\rangle\langle e| - |g\rangle\langle g|). \quad (S2)$$

Then, the effective frequencies for $|gn\rangle$ and $|en\rangle$ (the joint ancilla-cavity states) are $n\Delta\omega - n(n-1)\frac{K}{2} - \frac{\Omega^2}{(\Delta_d - n\chi)}$ and $n\Delta\omega - n(n-1)\frac{K}{2} + (\Delta_d - n\chi) + \frac{\Omega^2}{(\Delta_d - n\chi)}$, respectively. Therefore, the effective frequency for Fock state $|n\rangle$ is shifted by $\pm\frac{\Omega^2}{(\Delta_d - n\chi)}$ conditional on n and the state of the ancilla qubit. As a result, the detuned drive induces the PASS. For example, for the drive frequency lying between ancilla transition frequencies corresponding to $|n\rangle$ and $|n+1\rangle$, i.e. $\omega_q - (n+1)\chi < \omega_d < \omega_q - n\chi$, the PASS on $|gn\rangle$ and $|g(n+1)\rangle$ are negative and positive, respectively.

The PASS can also be understood from the point view of the geometric phase accumulated on the photonic Fock state due to the off-resonant drive, as shown in Fig. S2. The ancilla state initialized at the pole cannot be efficiently excited, but only rotates near the pole. The solid angle enclosed by the trajectory of the state on the Bloch sphere can be represented as

$$\Theta = 2\pi[1 - \cos(\theta)] = 2\pi(1 - \frac{\Delta}{\sqrt{4\Omega^2 + \Delta^2}}). \quad (S3)$$

For the detuned drive, the cycle period for the state rotating

on the Bloch sphere is

$$T_{\text{cyc}} = \frac{2\pi}{\sqrt{4\Omega^2 + \Delta^2}}, \quad (S4)$$

so the accumulated geometric phase ($\Theta/2$) is proportional to the number of rotation cycles, and the equivalent frequency shift can be derived as

$$\delta(\varepsilon, \Delta) = \frac{\Theta}{2T_{\text{cyc}}} = \frac{\sqrt{4\Omega^2 + \Delta^2} - \Delta}{2} \quad (S5)$$

$$\approx \frac{\Omega^2}{\Delta} \quad (S6)$$

for $|\Delta/\Omega| \gg 1$.

By taking into account the amplitude decay rate of the excited state of the ancilla qubit (κ_q), and for the ancilla prepared in the ground state, the effective Hamiltonian becomes

$$H_{\text{eff}} \approx \Delta\omega a^\dagger a - \frac{K}{2}a^{\dagger 2}a^2 - \frac{\Omega^2}{(\Delta_d - \chi a^\dagger a) - i\kappa_q}. \quad (S7)$$

Therefore, the PASS drive would not only induce the energy level shift

$$H_{\text{PASS}} = \sum_n \delta_n |n\rangle\langle n| = \sum_n \frac{\Omega^2}{\Delta_d - n\chi}|n\rangle\langle n|, \quad (S8)$$

but also induce the phase decoherence of the Fock states with a rate

$$\gamma_n \approx \frac{\Omega^2}{(\Delta_d - n\chi)^2}\kappa_q. \quad (S9)$$

This equation indicates that the frequency shift can be used to implement a logical-qubit phase gate while the error brought from the ancilla is significantly suppressed because of the ancilla's small excitation during the gate.

Here, we also want to briefly discuss the limitation of the PASS technique. For the purpose of error transparency in this work, the PASS should compensate the self-Kerr effect, i.e. $\delta_n = \mathcal{O}(K)$. If an individual PASS drive is applied to $|gn\rangle$ and $|g(n+1)\rangle$, we would have $\Delta_d - n\chi \approx \frac{\chi}{2}$, and thus the compensation requires $\frac{2\Omega^2}{\chi} = \mathcal{O}(K)$. In addition, the PASS requires a small drive amplitude $\Omega \ll \chi$ and negligible induced decoherence $\gamma_n \ll n\kappa_a$, with κ_a being the amplitude decay rate of the cavity. From Eq. (S9), we have $\gamma_n \approx \frac{4\Omega^2}{\chi}\frac{\kappa_q}{\chi} = \frac{2\kappa_q}{\chi}\mathcal{O}(K)$. Taking the fact that the self-Kerr coefficient of the cavity is related to the cross-Kerr coefficient (dispersive coupling strength) as $K = \chi^2/4E_c$, with E_c being the anharmonicity (the self-Kerr) of the ancillary transmon qubit, we can derive the conditions for the PASS drive to achieve the ET gates as: (1) $\Omega = \frac{\chi}{2}\mathcal{O}\left(\sqrt{\frac{\chi}{2E_c}}\right)$, (2) $\frac{1}{2}\sqrt{\frac{\chi}{2E_c}} \ll 1$, and (3) $\frac{\chi}{2E_c} \ll \frac{\kappa_a}{\kappa_q}$. For the device in this study, we have $E_c/2\pi \sim 252$ MHz, $\chi/2\pi \sim 1.60$ MHz and $\frac{\kappa_a}{\kappa_q} \sim 0.07$, therefore $\frac{\chi}{E_c} \sim 6.4 \times 10^{-3}$ and all the above conditions are satisfied. For a better performance of the PASS technique for ET gates, κ_q and $\frac{\chi}{E_c}$ of the superconducting circuit should be further reduced.

2. AQEC

AQEC is equivalent to the standard measurement-based QEC, which consists of both error detection and correction operations. However, AQEC does not need error detections. It is worth noting that the AQEC had been used with the three-qubit repetition code [7–9], while its extension to the bosonic codes requires rather sophisticated conditional unitary operations. To perform AQEC for the bosonic codes, a unitary transition is implemented to correct the logical state in the error space $|\psi_E\rangle$ while driving the ancilla to an orthogonal state:

$$U|\psi_E\rangle|g\rangle = |\psi_L\rangle|e\rangle, \qquad (S10)$$

but keep the logical state in the code space $|\psi_L\rangle$ unchanged:

$$U|\psi_L\rangle|g\rangle = |\psi_L\rangle|g\rangle. \qquad (S11)$$

In this case, the correlation between the quantum system and the environment (which induces errors) is erased, and thus the error entropy is transferred to the ancilla. After the operation, the logical state is recovered, and the ancilla system can be traced out. Note that in our experiment $|\psi_E\rangle = a|\psi_L\rangle$ (single-photon-loss error) in the error space; while there is a non-unitary no-jump evolution $e^{-\kappa_a a^\dagger a t/2}$ of $|\psi_L\rangle$ in the code space, which is corrected in the AQEC pulse.

In practice, we need to reuse the ancilla, therefore we reset the ancilla to a pure state after each implementation of AQEC for the next round of AQEC. Compared with previous demonstrations of QEC [10], the whole process does not need any projective measurement on the encoded bosonic state, and the error syndrome is not necessarily to be extracted. Therefore, the real-time feedback control system is not required any more and the potential electronic latency is avoided. The reset of the ancilla could be implemented in either digital or analog approaches. For the digital approach, the ancilla can be directly readout, and a control pulse dependent on the readout result is then applied to reset the ancilla. In this measurement-based case, the digital control only needs to implement the reset before the next AQEC step, which is hundreds of microseconds later in our case, in contrast to a few hundred nanoseconds required for real-time feedback control. For the analog approach, the ancilla could be engineered to couple to a readout cavity by switching on a stimulating drive, which can allow the decay of the excitation in the ancilla within about one microsecond. Here in this experiment, we use the so-called gradient ascent pulse engineering (GRAPE) algorithm [11, 12] to numerically optimize the AQEC pulse and use measurement-feedback method to reset the ancilla.

II. MORE EXPERIMENTAL DATA

A. Detailed experimental data of the PASS

In the experiment, we have used one or two microwave drives to precisely control the energy shifts of the photon number states, according to the photon-number-resolved AC-Stark
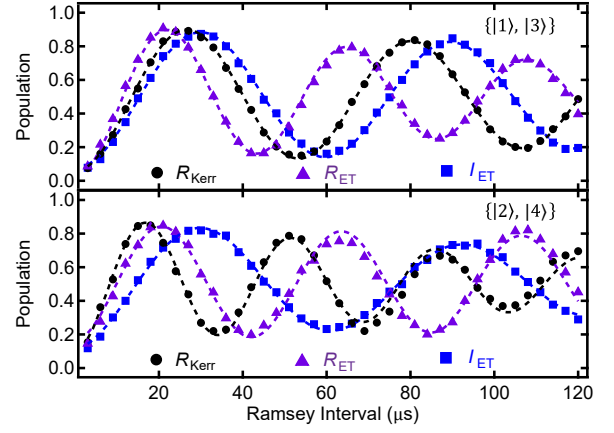

FIG. S3. **Ramsey-type experiments in the code and error spaces.** The Ramsey experiment is performed with a superposition of Fock states $|1\rangle$ and $|3\rangle$ (the error space basis); and Fock states $|2\rangle$ and $|4\rangle$ (the code space basis). The synchronized oscillations with both one and two PASS drives in the two spaces demonstrate the satisfaction of the ET condition. However, when the PASS drive is off, the oscillations are not synchronized any more, indicating the non-ET condition. The dashed lines are fits with a decayed sinusoidal function.

effect. The experimental technique and theoretical details are provided in the next section. Here, we show extra experimental results complementary to the presented ones in the main text.

Table S3 summarizes the parameters of the microwave drives used in the experiment. Δ_d is the drive detuning with respect to the ancilla qubit transition frequency when the cavity is in a vacuum state (i.e. there is no photon-induced frequency shift to the ancilla qubit), and Ω is the corresponding Rabi drive frequency that is proportional to the microwave driving amplitude. Here, all the driving parameters are optimized to minimize the excitation of the ancilla qubit in the simulation, and then carefully calibrated in the experiment.

For the ET phase gate, there is only one microwave drive with Δ_d being between -3χ and -4χ. Therefore, this drive makes the frequency shifts of Fock states $|3\rangle$ and $|4\rangle$ in opposite directions, thus satisfying the ET condition $(f_4 - f_2) - (f_3 - f_1) = 0$. Here f_n are measured through Ramsey-type experiments on superposition states $(|0\rangle + |n\rangle)/\sqrt{2}$ with $\Delta\omega = 0$. The experimentally measured f_n for the three different gates R_{Kerr}, R_{ET}, and I_{ET} are also provided in Table S3. We find that the ET condition is indeed satisfied. In comparison, the case without the PASS drive (the phase gate R_{Kerr} due to the Kerr coefficient) has $(f_4 - f_2) - (f_3 - f_1) \approx 2\pi \times 10$ kHz. For the ET gate R_{ET}, we choose a cavity frequency in a reference frame with $\Delta\omega/2\pi = 6.09$ kHz to fix the phase of Fock state $|4\rangle$, and then there is a non-zero rotating frequency of Fock state $|2\rangle$ relative to Fock states $|0\rangle$ and $|4\rangle$, i.e. $f_4/2 - f_2 = 6.67$ kHz. As a result, a phase gate can be realized to the binomial code.

By adding one more PASS drive with Δ_d being between

Driving parameter			ET phase gate				ET Idle	
Amplitude Ω			0.074χ				$0.054\chi, 0.074\chi$	
Detuning Δ_d			-3.41χ				$-3.37\chi, -2.27\chi$	

Fock state frequency shift (2π kHz)	$|1\rangle$	$|2\rangle$	$|3\rangle$	$|4\rangle$	$f_3 - f_1$	$f_4 - f_2$	$f_4/2 - f_2$
phase gate due to Kerr R_{Kerr}	0.14(3)	$-4.55(3)$	$-14.39(3)$	$-28.92(6)$	-14.25	-24.37	-9.91
ET phase gate R_{ET}	$-0.10(2)$	$-5.52(1)$	$-18.90(4)$	$-24.37(7)$	-18.80	-18.85	-6.67
ET idle gate I_{ET}	$-0.88(3)$	$-12.16(3)$	$-13.05(3)$	$-24.34(7)$	-12.17	-12.18	-0.02

TABLE S3. **Parameters of the PASS drives and frequency shifts in the experiment.** The numbers in the parenthesis are the measurement uncertainty.
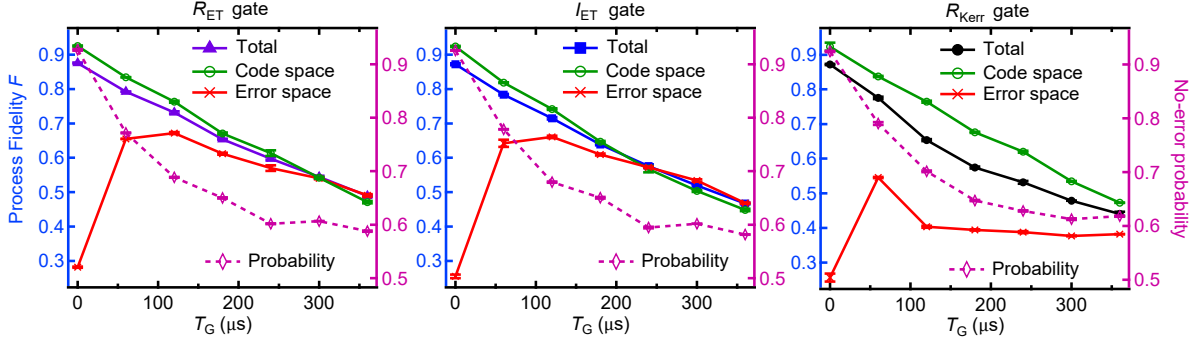

FIG. S4. **Process fidelity of the three single-logical-qubit gates with AQEC in the error space and code space respectively.** The dashed lines corresponding to the right vertical axis are the probabilities of detecting no-error (no single-photon loss).

-2χ and -3χ, we can further compensate the relative rotating frequency between $|0_L\rangle = (|0\rangle + |4\rangle)/\sqrt{2}$ and $|1_L\rangle = |2\rangle$, and essentially generate the ET idle gate I_{ET} in the same reference frame as R_{ET}. With the additional PASS drive, the induced frequency shifts of Fock states $|2\rangle$ and $|3\rangle$ have different directions. From Table S3, we find that $(f_4 - f_2) - (f_3 - f_1) = 0$ and $f_4/2 - f_2 = 0$ are both satisfied, indicating the satisfaction of both the ET condition and the idle operation condition. We note that such a gate is important for our experimental system, because the idle gate could be used to protect the quantum information together with QEC and the corruption of quantum information due to the Kerr effect can be eliminated.

The above ET/non-ET conditions with/without the PASS drives have been experimentally verified in Ramsey-type experiments, as shown in Fig. S3. The synchronized oscillations with one or two PASS drives in the code and error spaces demonstrate the satisfaction of the ET condition. However, when the PASS drive is off, the oscillations are not synchronized any more, indicating the non-ET condition.

B. Process fidelities for the single-logical-qubit gates with AQEC

Figure S4 provides more concrete data for the three different gates, accompanying Fig. 3 in the main text. The performances of the ET and non-ET gates are characterized by measuring the process fidelity F as a function of the gate time T_G. Here, F is separately measured for the code and error spaces by post-selecting the ancilla state that indicates if an error happens or not. The experimentally measured probabilities of no-error happening are also provided, by which the total fidelity can be derived as a weighted combination of those in both the error and code spaces.

The main feature for the three gates in Figure S4 is that the fidelities in the error space for the ET gates R_{ET} and I_{ET} are very similar and much higher than the non-ET gate R_{Kerr}. Such a difference manifests that the ET gates possess the capability of protecting the quantum information in the error space from corruption.

The no-error probability decays with T_G as expected, and so does the fidelity in the code space for all these three gates. However, the fidelities in the error space are low for $T_G = 0$, and then jump to a peak value followed by a decay. The reason for this unexpected behavior with small T_G is that in these cases the error is mainly induced by the ancilla decoherence, ancilla excitation, and operation errors, instead of the single-photon-loss error (has not happened yet) that the ET gates can protect. When T_G is large enough, the fidelity in the error space becomes much higher because the contribution of single-photon-loss errors dominates in the error space. When T_G further increases, the uncorrectable high-
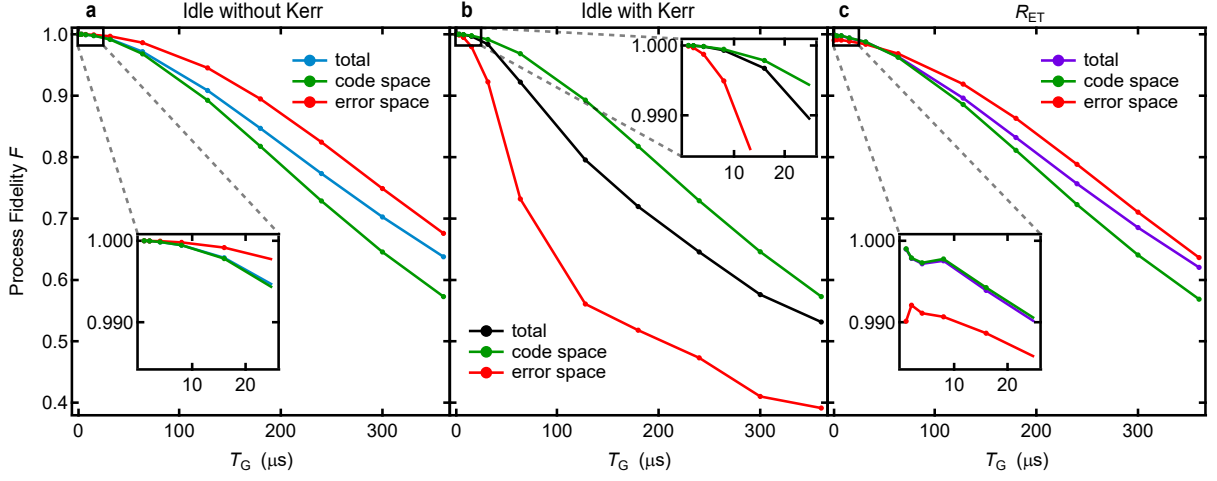
FIG. S5. **Numerical simulation results with ideal AQEC. a,** The ideal idle gate with no cavity's self-Kerr effect. **b,** The idle gate with cavity's self-Kerr effect. The logical state in the code space can still preserve, but corrupts quickly in the error space because the ET condition is not satisfied. **c,** ET phase gate with the PASS drive. The main trend is the same as **a** when T_G is sufficiently large. However, there is a little loss when T_G approaches zero because the effective Hamiltonian is no longer satisfied in this regime.
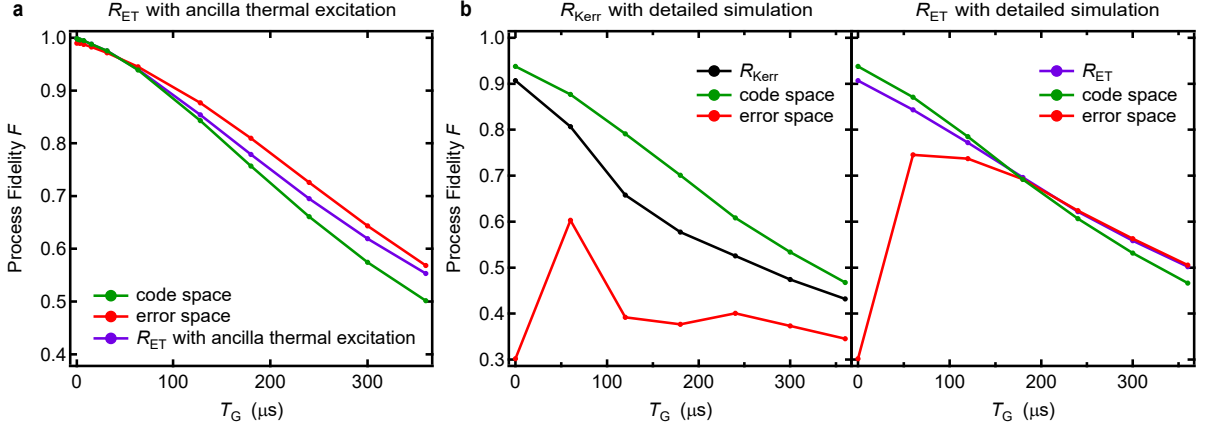

FIG. S6. **Numerical simulation results with ancilla thermal excitation and operation errors. a,** The ET phase gate with the ancilla thermal excitation, but still with ideal AQEC. The fidelity decays more linearly, in contrast to the quadratically decay curves in Fig. S5**c** with zero bath temperature. **b,** More detailed simulation of the non-ET phase gate R_{Kerr} and the ET phase gate R_{ET} including all possible imperfections. The results in **b** are very similar to the measured ones in Fig. 3**c** of the main text.

order photon-loss errors happen with higher probabilities, and therefore the overall fidelities in both the code and error spaces decay.

For the non-ET gate, the fidelity decays much faster because of the fast dephasing of quantum information in the error space due to the non-ET Kerr effect. Although the non-ET gate loses the phase information in the error space quickly, its fidelity remains at about 0.4 since the probability distribution of the basis states preserves, in good agreement with numerical simulations (see the numerical analysis below). It is also worth noting that the fidelities in the code space are slightly lower under the ET gates because of the additional ancilla excitation caused by the off-resonant drive (see the theory section for more discussions).

III. NUMERICAL ANALYSIS

To analyze sources of errors in the experiment and study the viability of the ET gates for potential fault-tolerant quantum computation, we implement numerical simulations according to our experimentally calibrated parameters. It is anticipated that the main experimental imperfections include: (1) the imperfect AQEC operations on the system, (2) the decoherence of the ancilla qubit during the ET gates, and (3) the thermal excitation of the ancilla qubit. In the following, we compare the results under different situations with the noiseless ideal case.

A. Numerical simulation with ideal AQEC

First of all, we use the ideal AQEC process in the numerical simulation to study the viability of the PASS technique for the realization of ET phase gates. The decoherence (damping and dephasing) of both the ancilla and the cavity are included in the numerical model. However, we assume the thermal bath are in the vacuum state, so the ancilla cannot be populated by the thermal noise from the bath. By substituting the experimentally calibrated parameters into the master equations, the system evolutions are numerically solved and the corresponding process fidelities are summarized in Fig. S5. Similar to the experiments in the main text, the ancilla qubit is traced out after the ET gate evolution with different gate times, and the density matrices in the error and code spaces are separately processed to obtain the process fidelities.

Comparing the results from the ET and non-ET gates in Fig. S5, we find the performances of the ET gates (Fig. S5**c**) are close to the ideal case without the cavity's self-Kerr effect (Fig. S5**a**). No self-Kerr effect of the cavity is a pre-assumption for many theoretical works on quantum gates [13]. However, when the self-Kerr presents in the cavity, the idle operation does not satisfy the ET condition, so the state in the error space corrupts quickly (Fig. S5**b**).

By applying the PASS technique on the system to engineer the Hamiltonian, the ET condition can be satisfied and the process fidelity in the error space preserves. However, we find that the curves of the ET phase gates are slightly lower than the ideal case. The reason could be attributed to the excitation of the ancilla by the off-resonant drive. As predicted by Eq. S9, the state jump of the ancilla qubit would induce the dephasing of the cavity states. In addition, there is a small loss of fidelity when T_G approaches zero (Fig S5**c** inset). This is because the effective Hamiltonian approximation for PASS is only satisfied when the gate time is sufficiently long $T_G \gg 1/\Delta$. Therefore, for $T_G < 10\,\mu$s in our experiment, the geometric phase cannot be regarded as continuously accumulated, and the PASS is deviated from Eq. S8.

B. Numerical simulation with ancilla thermal excitation and imperfect AQEC

The above simulations reveal the effect of the imperfections due to the drive-induced ancilla excitation and the consequent ancilla-excitation-induced dephasing, as predicted in the previous section on PASS. In practice, there are more imperfections that could induce the loss of gate fidelity.

One main contribution to the loss is the ancilla thermal excitation. The results including the ancilla thermal bath are shown in Fig. S6**a**. The fidelity decays more linearly, in contrast to the quadratically decay curves in Fig. S5**c** with zero bath temperature. As shown in Fig. S7, the ancilla excitation caused by the PASS drive increases with the drive amplitude. For the parameter used in our ET experiments ($\Omega/2\pi \sim 0.1$ MHz), the PASS-drive-induced excitation is smaller than
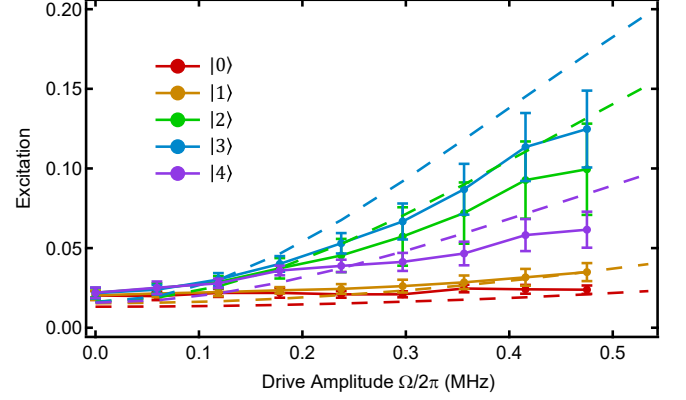

FIG. S7. **Ancilla excitation from the PASS drive.** The ancilla excitation due to an off-resonant drive with a detuning frequency $\Delta_d = -2.5\chi$ are measured as a function of the drive amplitude when the cavity is initialized at differnet Fock states. Dotted lines are simulation results. The ET gate used in the experiment is performed with the drive amplitude $\Omega/2\pi \approx 0.1$ MHz. Therefore, the additional excitation due to the PASS drive is about 0.01, while the thermal excitation is about 0.02.

the measured thermal excitation in the experiment. Therefore, we conclude that the photon dephasing is mainly from the ancilla thermal excitation, which can be suppressed by a cold bath. The PASS-drive-induced dephasing could be potentially solved by using alternative bosonic codes that are robust to dephasing errors, such as the cat code [14, 15] or the numerically optimized codes [16–18].

In the experiment, there are inevitable imperfections in the AQEC pulse and the measurement-feedback operation. To account for these errors on the performance of the non-ET gate R_{Kerr} and the ET phase gate R_{ET}, a more detailed simulation including these imperfections are carried out, and the results are shown in Fig. S6**b**. The obtained results agree well with the experimental results in Fig. 3 of the main text, indicating the main imperfections in our experiments are due to the thermal excitation of the ancilla qubit and the operation errors.

IV. THEORY

A. Requirement for error transparency

For an ET evolution, an error occurring at a random instant t should not affect the final output state except for an extra global phase, which can be represented by:

$$U(T,t)E_j U(t,0)|\psi_{\text{L}}\rangle = e^{i\phi(t)}E_j U(T,0)|\psi_{\text{L}}\rangle, \forall i,j,t. \quad \text{(S12)}$$

Here, $|\psi_{\text{L}}\rangle$ is an arbitrary logical quantum state in the code space, and E_j is in the error set. Because Eq. S12 should be satisfied for arbitrary time t, it is equivalent to

$$U(t+\delta t,t)E_j|\psi_{\text{L}}\rangle = e^{i\delta\phi(t)}E_j U(t+\delta t,t)|\psi_{\text{L}}\rangle. \quad \text{(S13)}$$

As a property of the logical gate, $U(t+\delta t,t)$ cannot introduce leakage out of the code space, i.e. $U(t+\delta t,t) = \mathscr{P}_C U(t+\delta t,t)\mathscr{P}_C$ with $\mathscr{P}_C$ being the projector onto the code space. Then the condition Eq. S13 can be transformed as

$$U(t+\delta t,t)E_j\mathscr{P}_C|\psi_L\rangle = e^{i\delta\phi(t)}E_j\mathscr{P}_C U(t+\delta t,t)\mathscr{P}_C|\psi_L\rangle, \tag{S14}$$

by adding the projectors. By combining the requirements for QEC

$$\mathscr{P}_C E_j^\dagger E_j \mathscr{P}_C = \alpha_j \mathscr{P}_C, \alpha_j \in \mathbb{R}, \tag{S15}$$

the ET condition becomes

$$\mathscr{P}_C E_j^\dagger U(t+\delta t,t)E_j\mathscr{P}_C = e^{i\delta\phi(t)}\alpha_j \mathscr{P}_C U(t+\delta t,t)\mathscr{P}_C. \tag{S16}$$

After introducing the projector $\mathscr{P}_j = \sqrt{\alpha_j}E_j\mathscr{P}_C$ from the code space to the error space due to E_j, the above equation becomes

$$\mathscr{P}_j^\dagger U(t+\delta t,t)\mathscr{P}_j = e^{i\delta\phi(t)}\mathscr{P}_C U(t+\delta t,t)\mathscr{P}_C. \tag{S17}$$

Since $U(t+\delta t,t) = I - iH(t)\delta t + \mathscr{O}(\delta t^2)$, the ET condition can also be represented by the system Hamiltonian as

$$\mathscr{P}_j^\dagger H(t)\mathscr{P}_j = \mathscr{P}_C H(t)\mathscr{P}_C + c(t)\mathscr{P}_C, \tag{S18}$$

where $c(t) = -d\phi(t)/dt$. Here, the Hamiltonian is presented in the code space.

In previous theoretical works [19, 20], the condition of ET gates is derived as

$$[E_j,H(t)]|\psi_{Li}\rangle = 0, \forall i,j,t. \tag{S19}$$

Comparing with the ET condition (Eq. S18) derived above, the commutation relation is too strict, and Eq. S19 is just equivalent to a special case of Eq. S18 with $\phi(t) = 0$. Therefore, the new ET condition provided in this work is more general with less restriction, and could relax the requirements for experimentally implementing the ET quantum gates.

* clzou321@ustc.edu.cn
† luyansun@tsinghua.edu.cn

[1] M. Reagor, W. Pfaff, C. Axline, R. W. Heeres, N. Ofek, K. Sliwa, E. Holland, C. Wang, J. Blumoff, K. Chou, M. J. Hatridge, L. Frunzio, M. H. Devoret, L. Jiang, and R. J. Schoelkopf, Phys. Rev. B **94**, 014506 (2016).

[2] C. Wang, Y. Y. Gao, P. Reinhold, R. W. Heeres, N. Ofek, K. Chou, C. Axline, M. Reagor, J. Blumoff, K. Sliwa, *et al.*, Science **352**, 1087 (2016).

[3] Y. Y. Gao, B. J. Lester, K. S. Chou, L. Frunzio, M. H. Devoret, L. Jiang, S. M. Girvin, and R. J. Schoelkopf, Nature **566**, 509 (2019).

[4] C. Axline, M. Reagor, R. Heeres, P. Reinhold, C. Wang, K. Shain, W. Pfaff, Y. Chu, L. Frunzio, and R. J. Schoelkopf, Appl. Phys. Lett. **109**, 042601 (2016).

[5] Y. Xu, W. Cai, Y. Ma, X. Mu, W. Dai, W. Wang, L. Hu, X. Li, J. Han, H. Wang, Y. Song, Z.-B. Yang, S.-B. Zheng, and L. Sun, arXiv:1810.04690 (2018).

[6] O. Gamel and D. F. V. James, Phys. Rev. A **82**, 052106 (2010).

[7] P. Schindler, J. T. Barreiro, T. Monz, V. Nebendahl, D. Nigg, M. Chwalla, M. Hennrich, and R. Blatt, Science **332**, 1059 (2011).

[8] M. D. Reed, L. DiCarlo, S. E. Nigg, L. Sun, L. Frunzio, S. M. Girvin, and R. J. Schoelkopf, Nature **482**, 382 (2012).

[9] G. Waldherr, Y. Wang, S. Zaiser, M. Jamali, T. Schulte-Herbrüggen, H. Abe, T. Ohshima, J. Isoya, J. F. Du, P. Neumann, and J. Wrachtrup, Nature **506**, 204 (2014).

[10] L. Hu, Y. Ma, W. Cai, X. Mu, Y. Xu, W. Wang, Y. Wu, H. Wang, Y. P. Song, C.-L. Zou, S. M. Girvin, L.-M. Duan, and L. Sun, Nat. Phys. **15**, 503 (2019), arXiv:1805.09072.

[11] N. Khaneja, T. Reiss, C. Kehlet, T. Schulte-Herbrüggen, and S. J. Glaser, J. Magn. Reson. **172**, 296 (2005).

[12] P. de Fouquieres, S. Schirmer, S. Glaser, and I. Kuprov, J. Magn. Reson. **212**, 412 (2011).

[13] V. V. Albert, K. Noh, K. Duivenvoorden, D. J. Young, R. T. Brierley, P. Reinhold, C. Vuillot, L. Li, C. Shen, S. M. Girvin, B. M. Terhal, and L. Jiang, Phys. Rev. A **97**, 032346 (2018).

[14] Z. Leghtas, G. Kirchmair, B. Vlastakis, R. J. Schoelkopf, M. H. Devoret, and M. Mirrahimi, Phys. Rev. Lett. **111**, 120501 (2013).

[15] M. Mirrahimi, Z. Leghtas, V. V. Albert, S. Touzard, R. J. Schoelkopf, L. Jiang, and M. H. Devoret, New J. Phys. **16**, 045014 (2014), arXiv:1312.2017.

[16] M. H. Michael, M. Silveri, R. T. Brierley, V. V. Albert, J. Salmilehto, L. Jiang, and S. M. Girvin, Phys. Rev. X **6**, 031006 (2016), arXiv:1602.00008.

[17] L. Li, C.-L. Zou, V. V. Albert, S. Muralidharan, S. M. Girvin, and L. Jiang, Phys. Rev. Lett. **119**, 030502 (2017), arXiv:1609.06386.

[18] L. Li, D. J. Young, V. V. Albert, K. Noh, C.-L. Zou, and L. Jiang, arXiv: 1901.05358 (2019).

[19] O. Vy, X. Wang, and K. Jacobs, New J. Phys. **15**, 053002 (2013).

[20] E. Kapit, Phys. Rev. Lett. **120**, 050503 (2018).